Trajectory Tracking of Mechanical Systems with Unilateral Constraints: Experimental Results of a Recently Introduced Hybrid PD Feedback Controller

Gian Paolo Incremona, Alessandro Saccon, Antonella Ferrara and Henk Nijmeijer

***Abstract*— The problem of tracking a time-varying reference trajectory of a mechanical system with unilateral position constraints is addressed in this paper. We present for the first time simulation and experimental results of a recently introduced trajectory tracking controller for hybrid systems with state jumps. The controller is applied to (locally) stabilize a time-varying trajectory of a 1-DOF robotic arm impacting and bouncing off an aluminum rod. The arm is modeled as a rigid link with viscous and Coulomb friction. The impact phenomenon is assumed to instantaneously reset the velocity in accordance with the classical Newton's law of restitution. Kinematic and dynamic identified parameter values are reported. The employed controller, hereafter called "hybrid PD controller with acceleration feedforward", requires the real time detection on each impact in order to properly define the error signal. To this end, a force sensor and a triggering logic based on a force threshold are employed.**

I. Introduction

Hybrid systems exhibit both continuous ("flow") and discrete ("jump") behaviors [1], [2]. Under suitable conditions, they may be used to describe the dynamics of mechanical systems with unilateral constraints, such as bipedal walkers [3], [4], juggling robots [5], or constrained mechanisms [6]. In this way, a trajectory tracking control problem for a mechanical system with unilateral constraint can be posed as a trajectory tracking control problem for a hybrid system with state-triggered jumps. A state-triggered jump corresponds, when considering the original mechanical formulation, to the occurrence of an impact between the mechanical system and the rigid obstacle defining the unilateral constraint [7].

Trajectory tracking of discontinuous state trajectories of a hybrid system is an active field of research [8]–[10]. We are interested in the specific situation when the jump times of the reference and the plant are different, similarly to what presented in [11] and [12]. A distinctive feature of [11] and [12] is the introduction of a new notion of tracking error, based on the idea of mirror reference trajectory. Further results in this direction include [12] and [13].

In [14], while addressing the same tracking problem studied in [11] and [12], the authors suggest the use of a new notion of tracking error, moving away from the concept of mirror trajectory. This work is a continuation of that line of thought. The new notion of error requires the (local) extension of the reference trajectory in each neighborhood of the nominal jump times. These extensions are referred to as extented ante- and post-event trajectories [14]. Further details about this control strategy and the synthesis of optimal gains can be found in [15].

Starting from the hybrid control law introduced in [14], this paper presents the first simulation and experimental results obtained by employing this hybrid controller for tracking a reference trajectory of a 1-DOF robot arm bouncing against an aluminum rod. Moreover, estimates of the coefficient of restitution obtained via experimental tests are also reported. After a standard least-square identification of the friction and inertia parameters, a reference trajectory is generated using Bézier curves to include the robot workspace constraints and the impact law. A suitable detection mechanism has been introduced by considering the comparison between contact force, exerted by the bouncing rod on an aluminum cylinder, and a pre-specified threshold, selected on the basis of experimental data. Numerical simulations show that the hybrid trajectory tracking controller employed in this work behaves effectively even when a compliant contact model (the Hunt and Crossley model [16], [17]), rather than a nonsmooth contact model, is employed.

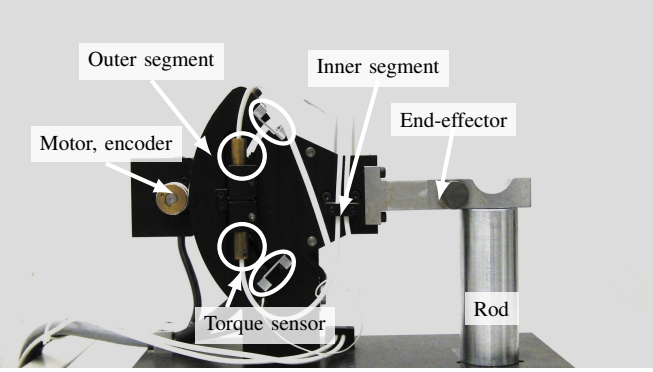

Fig. 1. The considered 1-DOF robotic setup and the aluminum rod: the torque sensor is made of two inductive sensors and two leaf springs that connect the outer with the inner segment.

II. The 1-DOF Setup: Modeling and Identification

The experimental setup used in this work is shown in Fig. 1. The setup consists of one rotational joint actuated by an electrical motor (design and construction details can be found in [18, Chapter 4]). The device presents two main segments,

This is the final version of the accepted paper submitted for inclusion in the Proceedings of the IEEE 54th Conference on Decision and Control, Osaka, Japan, Dec. 2015. Gian Paolo Incremona and Antonella Ferrara are with the Dipartimento di Ingegneria Industriale e dell'Informazione, University of Pavia, via Ferrata 1, 27100, Pavia, Italy. gp.incremona@gmail.com, antonella.ferrara@unipv.it

Alessandro Saccon and Henk Nijmeijer are with the Department of Mechanical Engineering, University of Technology, Eindhoven, the Netherlands. {a.saccon,h.nijmeijer}@tue.nl

one connected to the motor via a capstan drive (to reduce friction) and the other one fixed to the end-effector through two leaf springs. The relative displacement of the inner and outer segments, measured via a pair of inductive sensors, is used to obtain an estimation of the end-effector interaction force with the aluminum rod in steady state conditions (after a suitable calibration procedure). The position of the motor shaft $q(t)$ is measured by an incremental encoder with a resolution of 7500 pulses/revolution and a sampling rate of 2000 Hz. In the experimental work described in Section V, the impact of the end-effector on a solid object (the aluminum rod illustrated in Fig. 1) is studied.

A. Model Formulation

Following standard practice [19], [20], the 1-DOF setup is modeled as

$$J\ddot{q} + f_v\dot{q} + f_s\,\mathrm{sgn}(\dot{q}) = \Gamma, \tag{1}$$

where $q \in \mathbb{R}$ is the angular position, Γ is the actuation torque, J is the moment of inertia (including the motor and transmission), and f_v and f_s are, respectively, the viscous and Coulomb friction coefficients.

B. Identification of the Model Parameters

The identification procedure, based on the Least Square (LS) method, yielded the parameter values reported in the following table.

TABLE I
ESTIMATED PARAMETERS VALUES.

Param.	J [kg m^2]	f_v [N m s rad^{-1}]	f_s [N m]
Val.	1.493×10^{-3}	2.121×10^{-3}	3.906×10^{-3}

Remarkably, due to the quality of mechanical design, finite differentiation of the position signal is sufficient to obtain a good estimate of the velocity $\dot{q}$. The estimate of the acceleration $\ddot{q}$ has been obtained via a sliding mode based differentiator [21], [22]. The adopted Levant's differentiator, according to the sliding mode theory [23], [24], implies that robustness properties are enhanced with respect to some numerical or measurement disturbance. Specifically, one has

$$\begin{aligned} \dot{z}_0 &= -\lambda_0|z_0 - \dot{q}|^{1/2}\,\mathrm{sgn}(z_0 - \dot{q}) + z_1 \\ \dot{z}_1 &= -\lambda_1\,\mathrm{sgn}(z_0 - \dot{q}) \end{aligned} \tag{2}$$

where z_0 and z_1 are the estimated values of $\dot{q}$ and $\ddot{q}$, respectively, and $\lambda_0 = \Lambda^{1/2}$, $\lambda_1 = 1.1\Lambda$, $\Lambda \geq \sup|\ddot{q}|$, is a possible choice of the differentiator parameters [22].

C. Inverse Dynamics

The inverse dynamics controller [20]

$$\Gamma = Ju + f_v\dot{q} + f_s\,\mathrm{sgn}(\dot{q}) \tag{3}$$

with J, f_v, and f_s as in Table I and u the new virtual input has been employed to make the system behave as the simple double integrator

$$\ddot{q} = u \tag{4}$$

D. The Hybrid Model of the Plant

The 1-DOF arm can move freely as long as the unilateral position constraint

$$q \geq 0 \tag{5}$$

is satisfied. The constraint represents the surface of the aluminum cylinder. The dynamical model (4) is valid as long as $q > 0$. When $q = 0$ (and $\dot{q} < 0$), ideally the aluminum rod applies an impulsive force obtaining the velocity reversal

$$\dot{q}^+ = -e\dot{q}^- \tag{6}$$

where $e \in (0, 1]$ is the coefficient of restitution, while the superscripts $+$ and $-$ indicate the right and left limits of the velocity at the impact time.

Relying on the feedback linearized system (4), the corresponding state–space model is

$$\dot{x} = \begin{bmatrix} 0 & 1 \\ 0 & 0 \end{bmatrix} x + \begin{bmatrix} 0 \\ 1 \end{bmatrix} u \tag{7}$$

with $x = [x_1, x_2]^T := [q, \dot{q}]^T$ the system state.

The following section details the hybrid PD plus acceleration feedforward controller presented in [14] for the hybrid system with continuous dynamics (7) with guard map (5) and reset map (6).

III. THE HYBRID PD CONTROLLER

Adopting the notation in [14], we denote with $\tau \in [t_0, t_1]$ a jump time, f^- and f^+ the corresponding values of the vector field before and after the state reset. In terms of the state $x = (q, \dot{q})$, the unilateral constraint (5) is

$$g(x,t) := x_1 \geq 0. \tag{8}$$

Finally, the impact law (6) is rewritten as

$$x^+ = x^- + \Delta(x^-) \tag{9}$$

with $\Delta(x) = [0,\ -(1+e)x_2]^T$. Figure 2 depicts, as illustrative example, the trajectory of (7)-(9) corresponding to a coefficient of restitution $e = 0.4$ in the time interval $[1.5, 5]$ s. In the following, this state trajectory will be indicated with α and its corresponding input with μ. Together, (α, μ) represents the reference state-input trajectory that the hybrid system (7)-(9) has to track.

A. The State-Feedback Control Law

The state feedback control law proposed in [14] is

$$u(t) = \begin{cases} \mu(t) + K(\bar{\alpha}^a(t) - x(t)), & \text{before event detection} \\ \mu(t) + K(\bar{\alpha}^p(t) - x(t)), & \text{after event detection} \end{cases} \tag{10}$$

where $K = [K_P, K_D]$ is a PD control law. In (10), by "event detection" we mean the satisfaction of the condition $g(x(t),t) = 0$ for the current value of the state at time t. The novelty in the approach is the use of two reference signals in the proximity of each nominal event times. These so-called "extended ante-event" and "post-event state trajectories", $\bar{\alpha}^a(\cdot)$ and $\bar{\alpha}^p(\cdot)$, are obtained, respectively, by propagating the

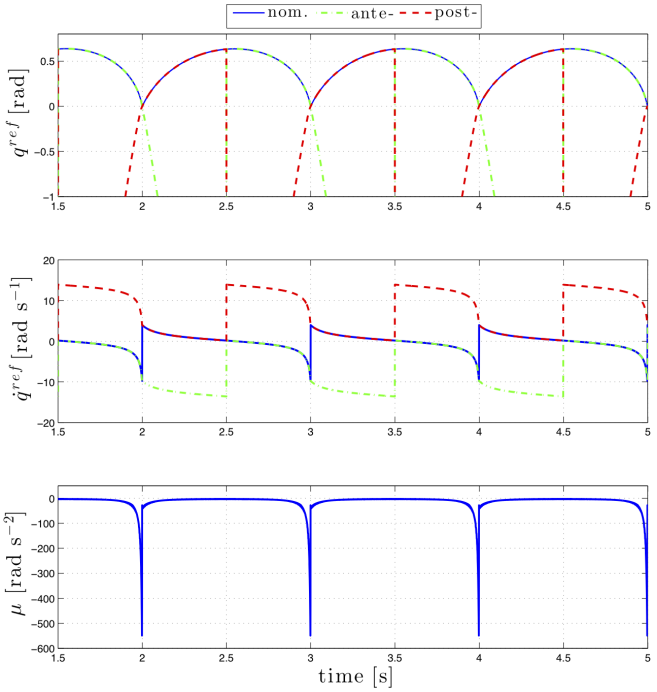

Fig. 2. Reference trajectories for position q^{ref} and velocity $\dot{q}^{ref}$ (nominal trajectory: solid blue line; "ante-event trajectory": dash-dotted green line; "post-event trajectory": dashed red line), and virtual input u to track.

nominal trajectory forward and backward in time from the nominal event times (about 2 s, 3 s, and 4 s, in Fig. 2) ignoring, during the integration of the equations of motion, the triggering condition $g(x,t)=0$. It suffices to compute the extended trajectories in a large enough neighborhood of the impact time (e.g., between $(\tau_i+\tau_{i+1})/2$ and $(\tau_{i+1}+\tau_{i+2})/2$, τ_i being the i-th event).

B. The Event Detection Mechanism

The detection of the impact events is based on the signals provided by the torque sensor. When the generalized force f_e on the cylinder exceeds a pre-specified threshold, an event counter is increased. The threshold has been decided according to specific experimental tests and the event counter is increased only when the force signal crosses the threshold in the rising direction.

IV. Estimating the Coefficient of Restitution

We discuss in this section the estimation of the coefficient of restitution e appearing in the reset map (6) or, equivalently, (9).

A. The Estimation Design

In order to perform the estimation of the restitution coefficient e, the 1-DOF setup has been driven to impact the aluminum cylinder at different velocities. Different values of the (virtual) input u, ranging from $100\,\mathrm{rad\,s^{-2}}$ to $500\,\mathrm{rad\,s^{-2}}$, have been applied, in open loop, to produce the impact.

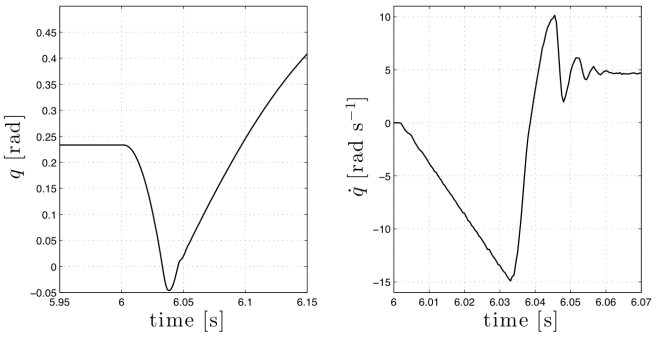

Fig. 3. Time evolution of the state trajectories in case of u =500 rad s^{-2}: from the left, the position q and the velocity $\dot{q}$.

B. Experimental Results

Figure 3 reports, as illustrative example, the impact data when the virtual control u is set to $500\,\mathrm{rad\,s^{-2}}$. Specifically, the motor position when impact occurs is illustrated together with the corresponding velocity profile. Note that, the velocity, obtained in the experimental test by using a constant acceleration, varies linearly and shows an abrupt velocity reversal in a fraction of a second. The restitution coefficient is computed by considering the mean value of the velocity after the event detection. It must be mentioned that differently from the idealized behavior, the experimental results show highly damped oscillations resulting from unmodeled internal flexibilities. Moreover, since the encoder is mounted on

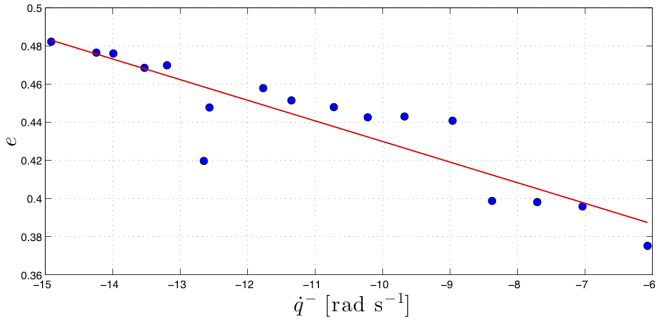

Fig. 4. Trend of the impact restitution coefficient e depending on the velocity value $\dot{q}^-$.

TABLE II
ESTIMATE OF THE IMPACT RESTITUTION COEFFICIENT.

$\dot{q}^-$ value	-6.0737	-7.0372	-7.7074	-8.3776
e value	0.3753	0.3958	0.3981	0.3988
$\dot{q}^-$ value	-8.9640	-9.6761	-10.2206	-10.7233
e value	0.4408	0.4430	0.4426	0.4479
$\dot{q}^-$ value	-11.3516	-11.7705	-12.5664	-12.6501
e value	0.4514	0.4579	0.4478	0.4197
$\dot{q}^-$ value	-13.1947	-13.5298	-13.9906	-14.9121
e value	0.4698	0.4685	0.4760	0.4822

the motor side which is separated from the segments, we obtain a negative value of q during the impact, although the corresponding end-effector position, which is not directly available, is expected to be equal to zero.

Table II reports the obtained results with respect to pre-impact velocity (i.e., the left limit of the velocity at the impact instant τ_c). A graphical representation of the same data is given in Fig. 4. Several tests have been performed to evaluate the repeatability of these results. Based on our experience, the obtained values, while being substantially unaltered between different trials, are however affected by the tensile preload of the cable that connects the outer segment with the capstan drive. It is our opinion that this explains the presence of the outliers in Fig. 4.

From this analysis, it has been decided to use e =0.4 as value for the coefficient of restitution to be used in the generation of the reference trajectory.

V. Tracking of a Time-Varying Reference Trajectory with State Jumps

In this section, simulation as well as experimental results obtained by applying the hybrid PD feedback controller are discussed.

A. The Reference Nominal Trajectory

Since the workspace of the considered 1-DOF setup is limited, the reference position trajectory has to satisfy specific bounds. Furthermore, the velocity trajectory has to be bounded

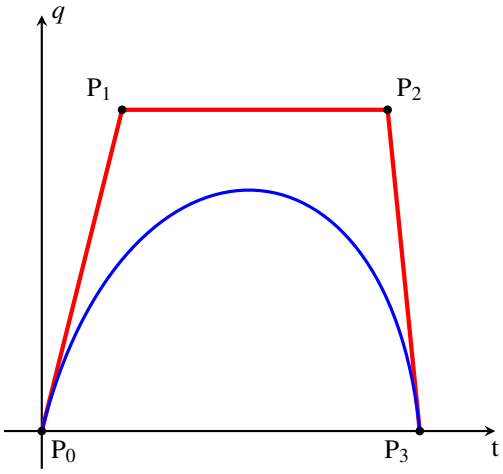

Fig. 5. Representation of a cubic Bezier curve guaranteed to lie within the polygon of its control points.

and it has to be consistent with the coefficient of restitution in a neighborhood of each impact time. Due to the specific setup at hand, the maximal displacement of the arm and its maximal velocity are q_{max} =0.85 rad and $\dot{q}_{max}$ =70 rad s^{-1}. We found that employing Bézier curves allows one to straightforwardly satisfy these constraints.

Bezier curves are guaranteed to lie within the polygon of its control points (see Fig. 5 for an illustrative example). In our case, the curve starts at $P_0 \equiv (t_0, q_0)$ going toward $P_1 \equiv (t_1, q_{max})$ and arrives at $P_3 \equiv (t_3, q_3)$ coming from the direction of $P_2 \equiv (t_2, q_{max})$. It does not pass through P_1 or P_2, but these points are necessary only to provide directional information, while the distance between P_0 and P_1 determines the curvature into direction P_2 before turning towards P_3. The

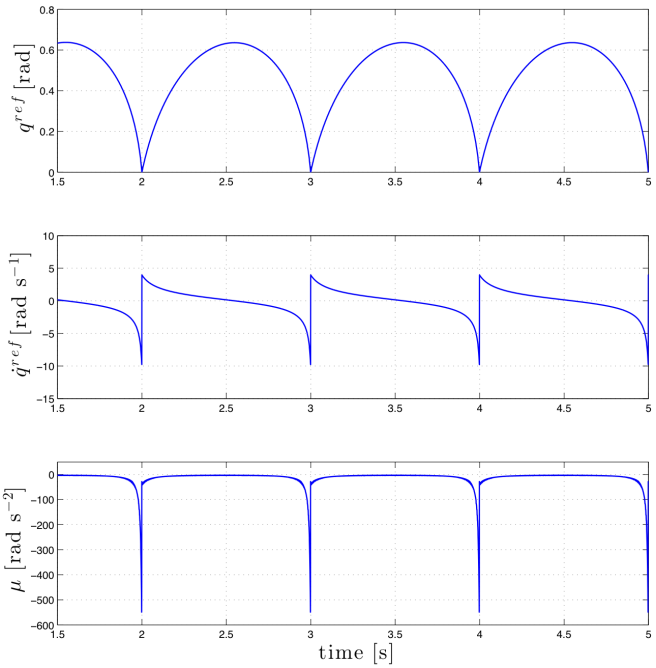

Fig. 6. Time-varying nominal reference trajectory with jumping state.

resulting nominal reference trajectory is reported in Fig. 6 with the position, the velocity and the acceleration profile.

B. PD Controller

As previously discussed, the control law chosen in (10) is of proportional-derivative type. Specifically, the parameters

TABLE III
PD control parameters.

K_P value	625
K_D value	70

reported in Table III have been set according to a conventional tuning method.

C. Simulation Results

In this section, the previously proposed hybrid controller is applied in simulation to the 1-DOF robot arm bouncing against the aluminum rod, using as model parameters those reported in Section II.

On purpose, we validate the control algorithm on a simulation model where the Hunt and Crossley contact model [16] has been used to compute the normal force which is exerted by the end-effector on the solid object. Specifically,

the contact force is

$$f_e = L \begin{cases} -k(z-H_f)+(z-H_f)\lambda\dot{z} & \text{if } z \le H_f \\ 0 & \text{if } z > H_f \end{cases} \quad (11)$$

such that

$$e = 1 - \frac{2}{3}\frac{\lambda}{k}\dot{q}^- \quad (12)$$

where $L = 0.165\,\mathrm{m}$ is the length of the arm, z is the lowest point of the end-effector, and H_f is the height of the aluminum cylinder. Moreover, $k = 8.8320 \times 10^4\,\mathrm{N\,m^{-1}}$ is the elastic coefficient chosen to match the value $e = 0.4$ found experimentally, while $\lambda = 5.2536 \times 10^4\,\mathrm{N\,s\,m^{-2}}$ is the damping factor. Note

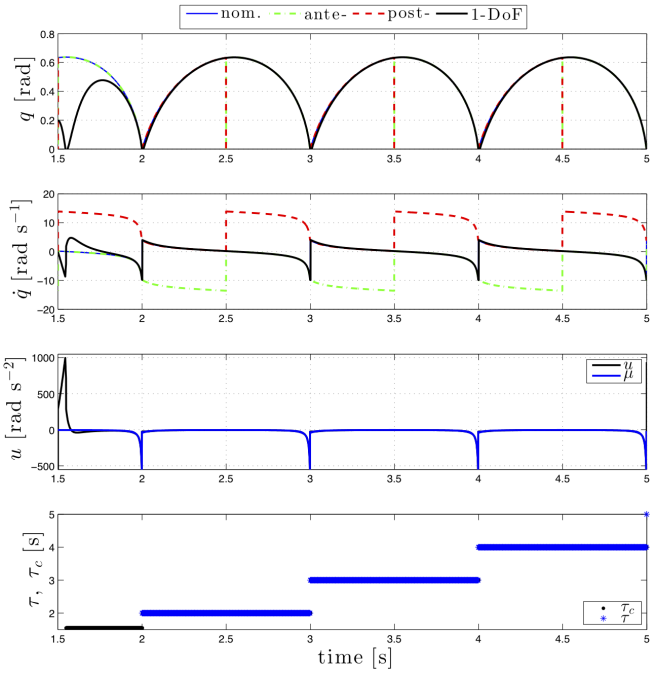

Fig. 7. Trajectory tracking of the controlled 1-DOF robot arm bouncing against the aluminum rod by using the hybrid PD control (simulation results).

that, since the 1-DOF robotic arm has a torque sensor, the generalized contact force f_e is expressed in N m. Figure 7 shows the time evolution of the state tracking the trajectory tailored to the specific 1-DOF setup. Specifically, position, velocity, input and event counter signals are illustrated. The simulation data corresponds to the solid black line, while the reference, post-, and ante-event extended trajectories are depicted, respectively, using a solid blue, dash-dotted green, and dashed red line.

D. Experimental Results

During experiments we have replicated the scenario considered in simulation.

Figure 8 depicts the position, velocity, input, and event counter signals. The experimental data corresponds to the solid black line. Figure 9 shows a close up about the impact time that occurs for t approximately equal to 3 s. In both Figures 8 and 9, the reference, post-, and ante-event extended

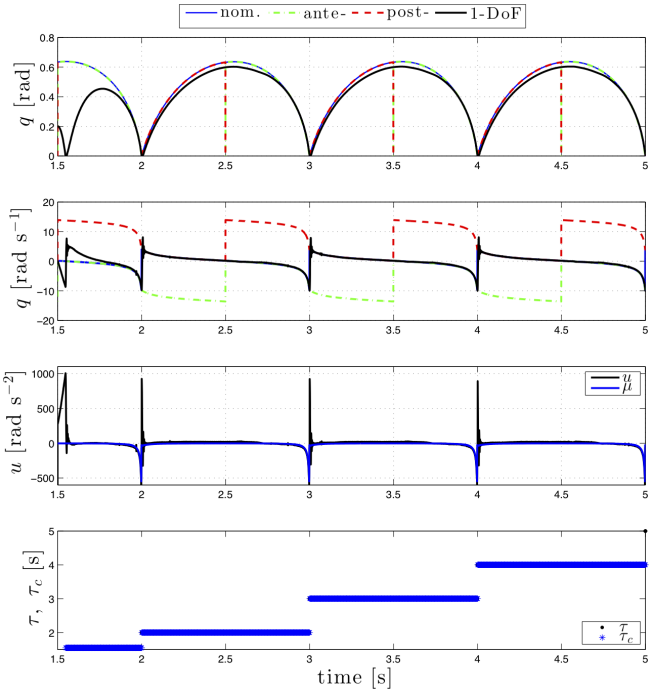

Fig. 8. Trajectory tracking of the controlled 1-DOF robot arm bouncing against the aluminum rod by using the hybrid PD control (experimental results).

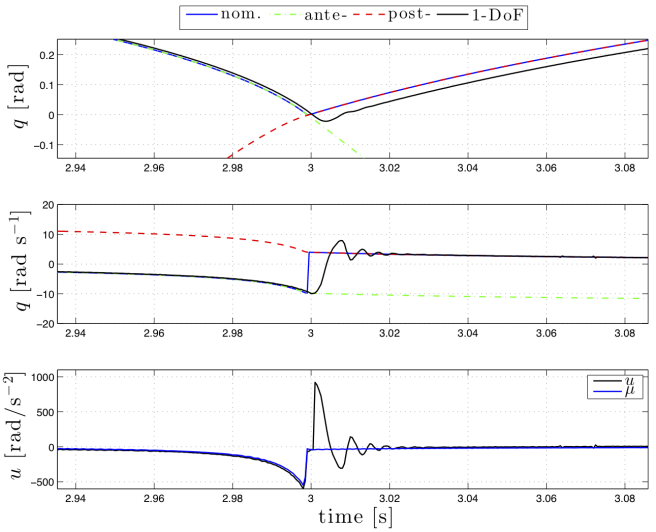

Fig. 9. Detail of the position, velocity and virtual control profile (experimental results).

trajectories are depicted, respectively, using a solid blue, dash-dotted green, and dashed red line. The contact force and the contact detection signal used to detect the impact occurrence are reported in Fig. 10.

The first thing to note is that the control strategy is capable of successfully stabilize the system about the desired trajectory. It is however evident that the tracking is not completely satisfying.

The unmodeled dynamics plays a crucial role in this experiments. Ideally, we should measure the position of the

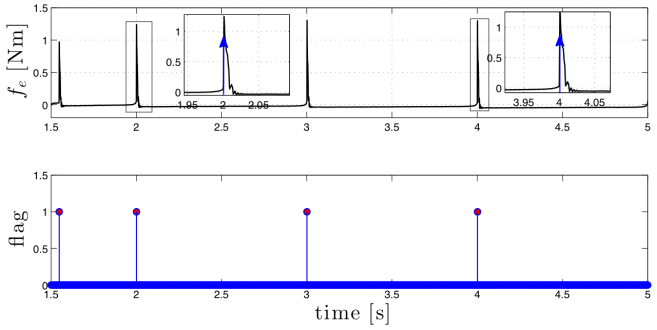

Fig. 10. Generalized force exerted by the end-effector on the object, and flag function equal to 1 when the contact event is detected (experimental results).

end-effector and use it in the computation of the tracking error. Currently, however, we can only measure the position of the motor shaft and therefore we find ourself in a situation which can be compared to the classical co-located control of a flexible joint, we sense and act on the motor side, but we have poor control of the load position. We are working on implementing an estimator of the tip position to improve this situation. The filtering effect of the unmodeled dynamics can be appreciated in the close up shown in Fig. 9.

VI. Conclusions

In this paper, the hybrid PD plus acceleration feedforward controller proposed in [14] has been tested on a real 1-DOF setup. Parameters values for the hybrid dynamical model, such as the viscous friction coefficient and the coefficient of restitution, have been identified with standard and ad hoc identification procedures. Simulations results, where the robot-environment interaction has been modeled using a Hunt and Crossley contact model and impact detection was obtained via the monitoring of the contact force magnitude, have shown that the hybrid PD controller with acceleration feedforward can be successfully applied even when impacts have finite time duration. A theoretical proof of robustness is still missing and needs further investigation. Experimental results have shown that unmodeled dynamics, probably related to a neglected structural mode, should be identified and included in the reference model to better predict the system behavior. Furthermore, the limited workspace of the current experimental setup created additional problems in the design of a suitable reference trajectory in accordance with the experimentally identified coefficient of restitution. The constrained motion planning problem was finally successfully addressed by employing a cubic Bézier curve. Despite of these limiting factors, the hybrid PD controller with acceleration feedforward has demonstrated the ability to successfully achieve stable tracking of trajectory with state jumps. A new experimental setup specifically designed to perform impact experiments as the ones described in this paper is under construction. This should allow for a better exploration and characterization of the performance of the proposed hybrid PD controller, removing the current hardware limitations.

References

[1] R. Goebel, R. Sanfelice, and A. Teel, *Hybrid Dynamical Systems: Modeling, Stability, and Robustness*. Princeton University Press, 2012.

[2] J. Lunze and F. Lamnabhi-Lagarrigue, Eds., *Handbook of Hybrid Systems Control: Theory, Tools, Applications*. Cambridge, UK: Cambridge University Press, 2009, ch. 1, pp. 4–30.

[3] E. R. Westervelt, J. W. Grizzle, and D. E. Koditschek, "Hybrid zero dynamics of planar biped walkers," *IEEE Trans. Autom. Control*, vol. 48, no. 1, pp. 42–56, Jan. 2003.

[4] B. Morris and J. W. Grizzle, "Hybrid Invariant Manifolds in Systems With Impulse Effects With Application to Periodic Locomotion in Bipedal Robots," *IEEE Trans. Autom. Control*, vol. 54, no. 8, pp. 1751–1764, Aug. 2009.

[5] R. Ronsse, P. Lefevre, and R. Sepulchre, "Sensorless stabilization of bounce juggling," *IEEE Trans. Robot.*, vol. 22, no. 1, pp. 147–159, Feb. 2006.

[6] S. Yadukumar, B. Kothapalli, and A. Ames, "Zeno behavior in electromechanical hybrid systems: From theory to experimental validation," in *IEEE American Control Conf.*, Montréal, Canada, Jun. 2012, pp. 2437–2442.

[7] B. Brogliato, *Nonsmooth Mechanics: Models, Dynamics and Control, Second edition*, ser. Communications and Control Engineering. Springer London, 1999.

[8] L. Menini and A. Tornambé, "Asymptotic tracking of periodic trajectories for a simple mechanical system subject to nonsmooth impacts," *IEEE Trans. Autom. Control*, vol. 46, no. 7, pp. 1122–1126, Jul. 2001.

[9] P. R. Pagilia and B. Yu, "An experimental study of planar impact of a robot manipulator," *IEEE/ASME Trans. Mechatronics*, vol. 9, no. 1, pp. 123–128, Mar. 2004.

[10] P. R. Pagilia, "Control of contact problem in constrained Euler-Lagrange systems," *IEEE Trans. Autom. Control*, vol. 46, no. 10, pp. 1595–1599, Oct. 2001.

[11] F. Forni, A. R. Teel, and L. Zaccarian, "Follow the Bouncing Ball: Global Results on Tracking and State Estimation With Impacts," *IEEE Trans. Autom. Control*, vol. 58, no. 6, pp. 1470–1485, Jun. 2013.

[12] J. J. B. Biemond, N. van de Wouw, M. Heemels, and H. Nijmeijer, "Tracking Control for Hybrid Systems With State-Triggered Jumps," *IEEE Trans. Autom. Control*, vol. 58, no. 4, pp. 876–890, Apr. 2013.

[13] J. J. B. Biemond, N. van de Wouw, M. Heemels, R. G. Sanfelice, and H. Nijmeijer, "Tracking control of mechanical systems with a unilateral position constraint inducing dissipative impacts," in *Proc. 51st IEEE Conf. Decision Control*, Maui, Hawaii, Dec. 2012, pp. 4223–4228.

[14] A. Saccon, N. van de Wouw, and H. Nijmeijer, "Sensitivity analysis of hybrid systems with state jumps with application to trajectory tracking," in *Proc. 53rd IEEE Conf. Decision Control*, Dec. 2014, pp. 3065–3070.

[15] M. Rijnen, A. Saccon, and H. Nijmeijer, "On optimal trajectory tracking for mechanical systems with unilateral constraints," in *Proc. 54rd IEEE Conf. Decision Control*, Osaka, Japan, Dec. 2015.

[16] K. H. Hunt and F. R. E. Crossley, "Coefficient of Restitution Interpreted as Damping in Vibroimpact," *Journal of Applied Mechanics*, pp. 440–445, Jun. 1975.

[17] N. Diolaiti, C. Melchiorri, and S. Stramigioli, "Contact impedance estimation for robotic systems," *IEEE Trans. Robot.*, vol. 21, no. 5, pp. 925–935, Oct. 2005.

[18] R. Hendrix, "Robotically assisted eye surgery: A haptic master console," Ph.D. dissertation, Technische Universiteit Eindhoven, Eindhoven, Netherlands, 2011.

[19] B. Siciliano and O. Khatib, Eds., *The Handbook of Robotics*. Berlin, Heidelberg, Germany: Springer, 2008, ch. 14, pp. 321–344.

[20] B. Siciliano, L. Sciavicco, L. Villani, and G. Oriolo, *Robotics-Modelling, Planning and Control*, 3rd ed. London, UK: Springer-Verlag, 2009, ch. 7, pp. 248–302.

[21] A. Levant, "Higher-order sliding modes, differentiation and output-feedback control," *Int. J. Control*, vol. 76, no. 9-10, pp. 924–941, Jan. 2003.

[22] ——, "Robust exact differentiation via sliding mode technique," *Automatica*, vol. 34, no. 3, pp. 379–384, Mar. 1998.

[23] V. I. Utkin, *Sliding Modes in Optimization and Control Problems*. New York: Springer Verlag, 1992.

[24] C. Edwards and S. K. Spurgeon, *Sliding Mode Control: Theory and Applications*. London, UK: Taylor and Francis, 1998.